Global and Planetary Change 144 (2016) 171–181

Contents lists available at ScienceDirect

Global and Planetary Change

journal homepage: www.elsevier.com/locate/gloplacha

Invited research article

Assessment of climate impacts on the karst-related carbon sink in SW China using MPD and GIS

Sibo Zeng [a,b], Yongjun Jiang [a,b,*], Zaihua Liu [c,*]

[a] School of Geographical Sciences, Southwest University, Chongqing 400715, China
[b] Karst Environment Laboratory, Southwest University, Chongqing 400715, China
[c] State Key Laboratory of Environmental Geochemistry, Institute of Geochemistry, Chinese Academy of Sciences, Guiyang 550081, China

ARTICLE INFO

Article history:
Received 5 January 2016
Received in revised form 24 July 2016
Accepted 28 July 2016
Available online 29 July 2016

Keywords:
Karst-related carbon sink
Climate change
MPD
GIS
SW China

ABSTRACT

Riverine carbon fluxes of some catchments in the world have significantly changed due to contemporary climate change and human activities. As a large region with an extensive karstic area of nearly 7.5×10^5 km^2, Southwest (SW) China has experienced dramatic climate changes during recent decades. Although some studies have investigated the karst-related carbon sink in some parts of this region, the importance of climate impacts have not been assessed. This research examined the impacts of recent climate change on the karst-related carbon sink in the SW China for the period 1970–2013, using a modified maximal potential dissolution (MPD) method and GIS. We first analyzed the major determinants of carbonate dissolution at a spatial scale, calculated the total karst-related carbon sink (TCS) and carbon sink fluxes (CSFs) in the SW China karst region with different types of carbonate rocks, and then compared with other methods, and analyzed the causes of CSFs variations under the changed climate conditions. The results show that the TCS in SW China experienced a dramatic change with regional climate, and there was a trend with TCS decreasing by about 19% from 1970s to 2010s. This decrease occurred mostly in Guizhou and Yunnan provinces, which experienced larger decreases in runoff depth in the past 40 years (190 mm and 90 mm, respectively) due to increased air temperature (0.33 °C and 1.04 °C, respectively) and decreased precipitation (156 mm and 106 mm, respectively). The mean value of CSFs in SW China, calculated by the modified MPD method, was approximately 9.36 t C km^{-2} a^{-1}. In addition, there were large differences in CSFs among the provinces, attributed to differences in regional climate and to carbonate lithologies. These spatiotemporal changes depended mainly on hydrological variations (i.e., discharge or runoff depth). This work, thus, suggests that the karst-related carbon sink could respond to future climate change quickly, and needs to be considered in the modern global carbon cycle model.

1. 1. Introduction

Atmospheric CO_2 plays a significant role in controlling global climate. The established global carbon cycle models, however, cannot balance the atmospheric CO_2 budget, leaving a so-called "missing carbon sink" problem (Tans et al., 1990; Melnikov and O'Neill, 2006). Finding the missing carbon sink is becoming one of the most important questions in the research of global climate change. Although the weathering of silicate minerals can capture atmospheric CO_2 by forming HCO_3^- from continent to oceans (Berner et al., 1983; Berner, 1992), this carbon sink is limited due to the slow weathering kinetics of silicate minerals over short time scales (Liu et al., 2011). Carbonate rock is the world's biggest carbon reservoir, and the rapid kinetics of carbonate dissolution result in a large amount of atmospheric CO_2 consumption (Yuan, 1997; Liu and Zhao, 2000; Gombert, 2002; Liu et al., 2010; Liu et al., 2011). Furthermore, according to a new conceptual model of the carbon sink produced by H_2O-carbonate-CO_2-aquatic phototroph interaction, this carbon sink produced by carbonate weathering can be transferred by aquatic organisms and buried as organic matter (Liu and Dreybrodt, 2015). Therefore, carbonate weathering coupled with aquatic photosynthesis are a significant potential mechanism for the terrestrial missing carbon sink (Liu and Dreybrodt, 2015).

The increase in atmospheric CO_2 has resulted in remarkable contemporary global climate change (Friedlingstein et al., 2006, Gedney et al., 2006), but the carbon sink produced by chemical weathering of rocks has been considered to be unchanged since pre-industrial times in global carbon models (Sabine et al., 2004). However, recent investigations have found evidence that contemporary climate change is accelerating the chemical weathering rate and altering the relevant carbon fluxes (Raymond and Cole, 2003; Macpherson et al., 2008; Raymond et al., 2008; Gislason et al., 2009). Duo to the high sensitivity of carbonate weathering to environmental change (Liu et al., 2007; Yang et al., 2012), the response of this carbon sink may be rapid and considerable (Liu and Dreybrodt, 2015; Zeng et al., 2016). For instance, Raymond et al. (2008) and Raymond and Cole (2003) attributed a proximately 20%

* Corresponding authors.
E-mail addresses: jiangjyj@swu.edu.cn (Y. Jiang), liuzaihua@vip.gyig.ac.cn (Z. Liu).

http://dx.doi.org/10.1016/j.gloplacha.2016.07.015
0921-8181/

increase of alkalinity ($HCO_3^- + CO_3^{2-}$) (increasing from 20.3 mg/L to 25.4 mg/L) in the Mississippi River during the past half-century to a 9% increase in precipitation. Macpherson et al. (2008) found a 20% increase in groundwater pCO_2 and 13% increased alkalinity between 1990 and 2005 in the karst area of Konza Prairie, USA, due to the increasing atmospheric CO_2 and perhaps atmospheric temperature. An experimental air CO_2 enrichment study in Duke Forest also indicated that an elevated atmospheric CO_2 experiment of 200 ppm (+50%) in two years led to 33% increase in alkalinity of ground water duo to accelerating chemical weathering (Andrews and Schlesinger, 2001). Therefore, it is problematic that the conventional assumption that pre- and post- anthropogenic riverine carbon fluxes are the same (Sabine et al., 2004), and it is necessary to quantify the strength of the feedback of the karst-related carbon sink to changed climate conditions worldwide.

Many methods have been used to calculate the global karst-related carbon sink, including the DBL (Diffusion Boundary Layer) model (Liu and Zhao, 2000) and the MPD (Maximal Potential Dissolution) formula (Gombert, 2002). The MPD formula is a theoretical method based on climatic parameters. The calculations of MPD could be a powerful tool when used to estimate karst-related carbon sink perturbations due to changed climate conditions (Gombert, 2002). On the other hand, consideration of carbonate lithologies (limestone and dolomite) in estimating the karst-related carbon sink in a large karstic area is critical, due to their different solubilities (Dreybrodt, 1988).

The primary objective of this paper is to assess the karst-related carbon sink response to the changed climate over the past 40 years in SW China, where there is a high percentage (~43%) of karstic area with different carbonate lithologies and there is a monsoonal climate, using the MPD and GIS.

2. 2. Study area

The study area is situated in SW China (20°54′–34°19′ N, 97°21′–116°08′ E) (Fig. 1), covering approximately 17.6×10^5 km^2 and including seven provinces: Sichuan, Chongqing, Hubei, Yunnan, Guizhou, Hunan and Guangxi. The northwestern and eastern sides of the study area are bordered by the Tibet Plateau and the Central China Plain, respectively, and thus the altitude is higher in the west (Fig. 1). The karst region of SW China is well known for its extensive carbonate rock outcrop and intensive karst landform development. Plateaus, mountains and plains are the main landform types in the region, and the area is characterized by typical monsoonal climate. Annual precipitation in the area is about 1148 mm, most of which falls in the monsoon season from April to September. The mean annual air temperature in SW China is about 15.4 °C, with hot summers (June–August) and cold winter (December–February) (http://cdc.cma.gov.cn).

3. Methods

3.1. Data collection

The distribution of karst in SW China was extracted from maps of soluble rock types in China, as edited by Institute of Karst Geology, Chinese Academy of Geological Sciences (1985). By calculation and classification, the karst region in SW China covers an area of approximate 7.5×10^5 km^2 and the main lithologies include limestone, dolomite, mixed limestone/dolomite and impure carbonate rocks mixed with clays or other silicate minerals (Fig. 2). The areas underlain by karst in each province are shown in Table 1.

Daily meteorological data, including precipitation (P, mm), mean temperature (T_{mean}, °C), insolation duration (n, h), mean humidity (RH_{mean}, %), and mean wind speed (WS, m/s), in 240 stations in and around the SW China from 1970 to 2013 (data from 1981, 1982 and 1984 are missing) (station locations are shown on Fig. 1), were obtained from the China Meteorological Data Sharing Service System (http://cdc.cma.gov.cn).

3.2. Maximal potential dissolution (MPD) method

Many methods can be used to calculate the carbonate dissolution rate. However, most of these methods need long-term field measurements or complicated parameters which are difficult to obtain, which

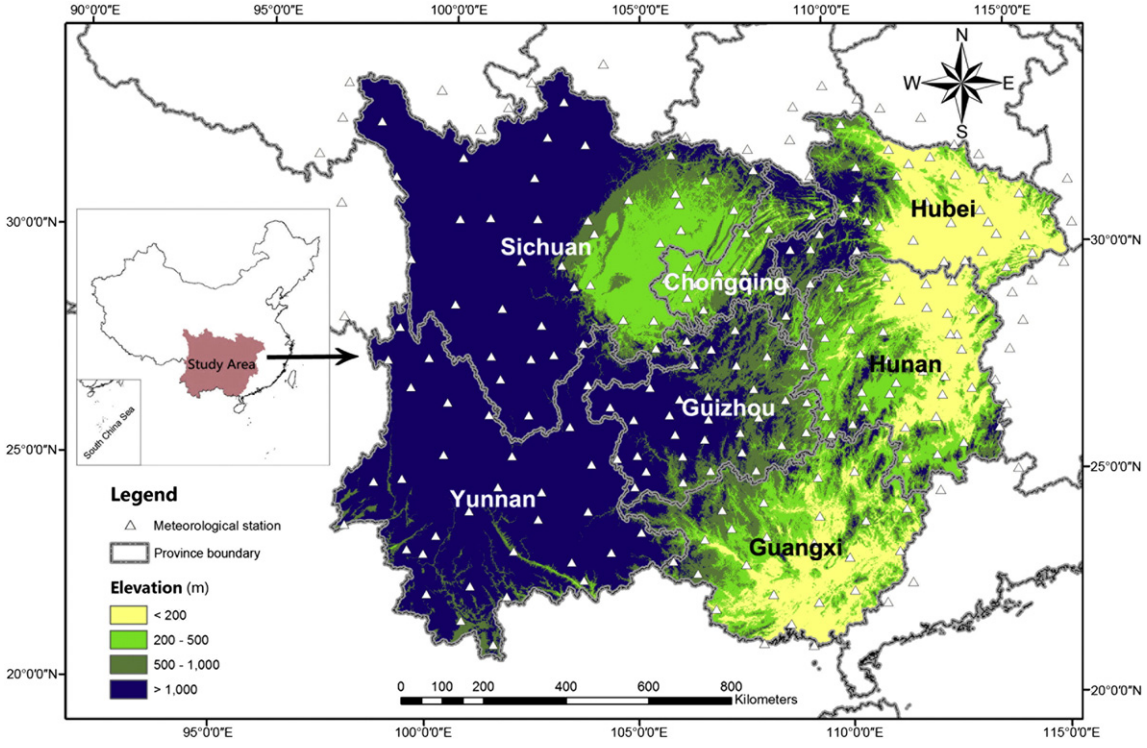

Fig. 1. Location of SW China and the distribution of meteorological stations in the area (modified after http://cdc.cma.gov.cn).

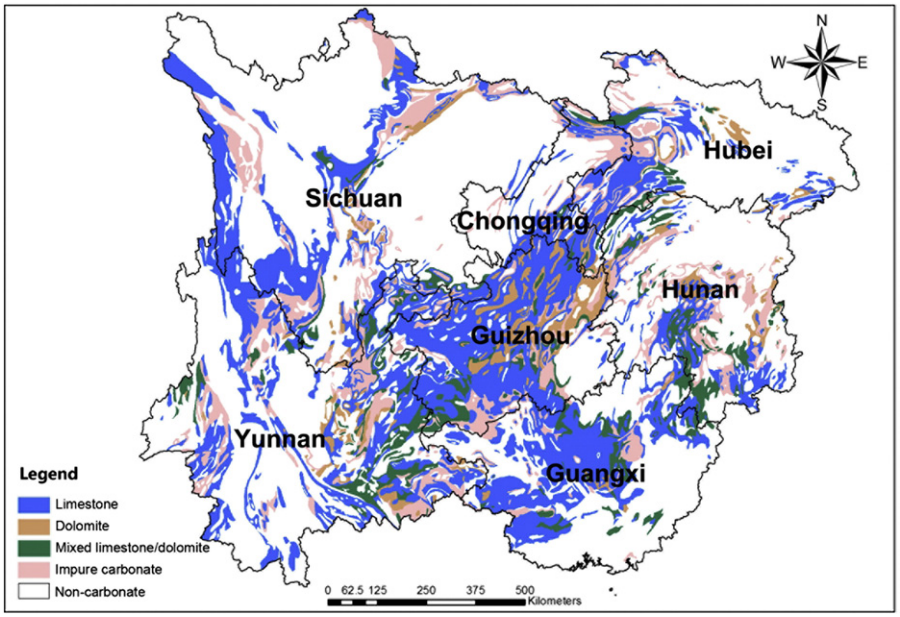

Fig. 2. Distribution of various carbonate rocks in SW China (modified after the Institute of Karst Geology, Chinese Academy of Geological Sciences, 1985).

makes it difficult to estimate the response of the karst-related carbon sink to climate change in a large karst area. To solve these problems, Gombert (2002) created a theoretical method optimizing carbonate dissolution processes called Maximal Potential Dissolution (MPD). The intensity of karstification and the relevant carbon sink can be obtained by the MPD method, if air temperature, precipitation, evapotranspiration are known in the given area.

Gombert (2002) gave the usual equation for dissolution of calcite at equilibrium:

$$CaCO_3 + CO_2 + H_2O \leftrightarrow Ca^{2+} + 2HCO_3^-$$

The equation equilibrium constant K^* can be expressed as:

$$K* = \left(Ca^{2+}\right)(HCO_3^-)^2/(CO_2) = K_s(K_1/K_2),$$

where parentheses correspond to activities; K_1 is the equilibrium constant of the CO_2 hydration and dissociation with the formation of HCO_3^-; K_2 is the equilibrium constant of CO_3^{2-} formation; and K_S is the calcite solubility constant. The value of (CO_2) can be obtained by using Henry's law:

$$(CO_2) = K_0 pCO_2,$$

where K_0 is the equilibrium constant of CO_2 dissolution in water, and pCO_2 is the partial pressure of CO_2 inside the soil or aquifer.

When the reaction maintains equilibrium, we have:

$$2\left[Ca^{2+}\right] = [HCO_3^-]$$

K^* is thus:

$$K* = 4\left[Ca^{2+}\right]/(K_0 pCO_2) = K_s(K_1/K_2)$$

Hence, at $CaCO_3$ saturation, Ca^{2+} concentrations can be expressed as:

$$\left[Ca^{2+}\right]_{eq} = (K_s K_1 K_0/4K_2)^{1/3}(pCO_2)^{1/3}$$

MPD's mathematical formulation of the maximal theoretical dissolution flux (mol $km^{-2}\cdot a^{-1}$) incorporates this equilibrium calcite dissolution with climate parameters:

$$D_{max} = 10^6(P\text{-}E)\left[Ca^{2+}\right]_{eq} = 10^6(P\text{-}E)\left(K_s K_1 K_0/4K_2\gamma_{Ca}\gamma_{HCO3}{}^2\right)^{1/3}(pCO_2)^{1/3}$$

where P is the total precipitation (mm/a); E is the evapotranspiration (mm/a); $[Ca^{2+}]_{eq}$ is the concentration of calcium for calcite at equilibrium; γ_{Ca},γ_{HCO3} are activity coefficients of Ca^{2+} and HCO_3^- in water, respectively.

The dissolution of each mole of $CaCO_3$ consumes one mole CO_2. Thus, according to MPD, the karst-related carbon sink fluxes can be calculated by the following equation:

$$CSFs = 10^6(P\text{-}E)[HCO_3^-]_{eq}/2 = 10^6(P\text{-}E)\left[Ca^{2+}\right]_{eq} = 10^6(P\text{-}E)\left(K_s K_1 K_0/4K_2\gamma_{Ca}\gamma_{HCO3}{}^2\right)^{1/3}(pCO_2)^{1/3} \quad (1)$$

The annual total carbon sink (TCS, t C a^{-1}) in a given karst area can then be expressed as follow equation:

$$TCS = 6DS[HCO_3^-]_{eq} \quad (2)$$

where D is the runoff depth (P-E) (m/a), S is the land surface area underlain by karst (km^2), and $[HCO_3^-]_{eq}$ is the concentration of bicarbonate for calcite at equilibrium (mmol/L).

Table 1
Karstic areas of the seven provinces in SW China.

Province	Yunnan	Guizhou	Sichuan	Guangxi	Huanan	Hubei	Chongqing	Total
Karstic area ($10^4\cdot km^2$)	19.1	14.5	14.0	10.3	8.2	5.9	3.2	75.2

3.3. An extension of MPD method to other type of carbonates

In natural conditions, other types of carbonates than calcite also exist. Dolomite is 21%–38% more soluble than calcite at temperatures between 0 and 30 °C (Fig. 3; Dreybrodt, 1988; Liu et al., 2007), indicating that the carbonate lithology may play a significant role in controlling the size of the karst-related carbon sink flux. In order to distinguish the differences in equilibrium concentration between multiple types of carbonates, an equilibrium concentration calculating software EQILCAMG (Dreybrodt, 1988) was used to determine the ratio of the moles of calcite and dolomite that will dissolve at equilibrium [$C(eq)_D/C(eq)_L$] as a function of temperature (Fig. 3), which is found to be linear as:

$$y = -0.571x + 139.08 \quad (3)$$

Eq. (3) was then used to calculate the equilibrium concentration of dolomite dissolution in SW China when calculating the dolomite karst-related carbon sink with the MPD method.

3.4. Calculation of runoff depth and evapotranspiration (ET)

In MPD formula Eq. (2), the runoff depth (D) in the study area results from effective precipitation (P_e), which is calculated as annual precipitation (P) minus actual evapotranspiration (ET). The Penman-Monteith is a reliable and accurate accepted model based on metrological parameters, and has been applied to estimate reference evapotranspiration (ET_0) under climate change. In this study, the daily ET_0 was calculated from a radiation corrective FAO56 Penman-Monteith model and the results were assumed to be equal to actual evapotranspiration (ET) at each meteorological station in SW China. This can be expressed by the following equation (Allen et al., 1998):

$$ET_0 = \frac{0.408\Delta(R_n - G) + \gamma\frac{900}{T+273}U_2(e_s - e_a)}{\Delta + \gamma(1 + 0.34U_2)} \quad (4)$$

where ET_0 is the reference evapotranspiration (mm d^{-1}); R_n is the net radiation at the crop surface (MJ m^{-2} d^{-1}); G is the soil heat flux density (MJ m^{-2} d^{-1}) (at daily scale it is negligible, $G_{day} = 0$); T is the mean daily air temperature at a height of 2 m (°C); U_2 is the wind speed at a height of 2 m (m/s); e_s is the saturation vapor pressure curve (kPa/°C); e_a is the actual vapor pressure; Δ is the slope vapor pressure curve (kPa/°C), and r is the psychometric constant (kPa/°C). In order to obtain the reference evapotranspiration more accurately in the study area, a radiation calibration in China by Yin et al. (2008) was adopted.

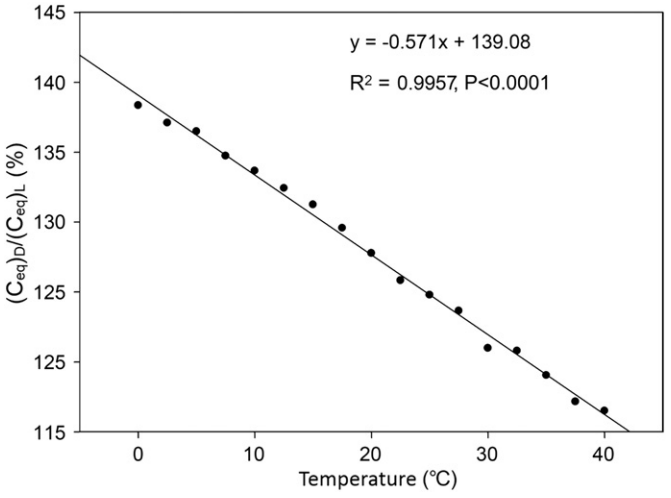

Fig. 3. Correlation between $(Ceq)_D/(Ceq)_L$ and temperature. $(Ceq)_D$ and $(Ceq)_L$ are equilibrium concentrations of bicarbonate for dolomite and limestone, respectively.

3.5. 3.5. Soil pCO_2 calculation

Soil CO_2 is a key driving force of karst processes and related carbon sequestration (Yang et al., 2012; Zeng et al., 2016), because the soil CO_2 concentration is about 10 to 100 times higher than that in the atmosphere (Drever, 1994). Also, the CO_2 partial pressure (pCO_2) in groundwater is mainly determined by the soil pCO_2. Thus, pCO_2 in groundwater can be supposed to be equilibrated with an actual soil pCO_2 in this study, and calculated from Brook et al. (1983) formula in the MPD:

$$\log(pCO_2) = -3.74 + 2.09\left(1 - e^{-0.00172AET}\right) \quad (5)$$

where pCO_2 is the partial pressure of CO_2 (atm) in soil, AET is the annual actual evapotranspiration (ET) during the growing period (mm/a). In this study, AET was assumed to be equal to the ET_0 calculated from the section 3.4.

3.6. Spatial and temporal analysis of CSFs and TCS

In order to reveal the spatial distribution of CSFs in SW China, the annual precipitation, evapotranspiration, equilibrium bicarbonate concentration across the SW China were determined by ordinary Kriging interpolation in ArcGIS 9.3. In this Study, the CSFs and *TCS* of SW China were calculated from 1 km × 1 km grids through GIS spatial analysis.

Decadal averages were used to calculate and map the CSFs changes from 1970 to 2013. For example, the 1970s represents the period of 1970 to 1979, the 1980s for 1980–1989, the 1990s for 1990–1999, the 2000s for 2000–2009, but the 2010s only for four years from 2010 to 2013. The response and trend of each factor to changed climate conditions were obtained by linear regression analysis.

4. Results

4.1. Spatial – temporal changes in climate in SW China

Fig. 4 shows the changes in annual mean temperature, net total radiation, wind speed, precipitation and evapotranspiration (ET) for the period of 1970–2013 from 240 meteorological stations in SW China (Fig. 1). An increasing trend of temperature was observed by the linear regression model during the study period, with a slope of 0.025 °C/a (Fig. 4). Precipitation showed a significant decreasing trend with slopes of −1.7 mm/a in the study period (Fig. 4). Although ET, net total radiation and wind speed demonstrated increasing trends from 2003 to 2013, the significant decreasing trends of these indexes were observed during the whole study period, with slopes of −0.2 mm/a, −2.8 MJ Day^{-1} $m^{-2}a^{-1}$ and −0.0068 m/sa^{-1}, respectively (Fig. 4). Furthermore, precipitation fluctuated more than ET: the highest precipitation value (1345 mm) occurred in 2002 and the lowest in 2011 (963 mm), while the highest ET occurred in 2013 (837 mm) and the lowest (716 mm) in 1993.

Fig. 5 shows the spatial changes and temporal trends of mean temperature and precipitation in SW China from 1970s to 2010s. The mean value of temperature and precipitation in SW China were 15.4 °C and 1147 mm/a, respectively. During the whole study period, the provinces with the largest increasing trends of temperature were Sichuan and Yunnan (0.22 and 0.26 °C/decade, respectively), as shown in Fig. 5(c). However, Yunnan and Guizhou provinces showed the largest decrease in precipitation (Fig. 5(c)), with −24.1 mm/decade and −37.4 mm/decade, respectively. Most provinces demonstrated decrease in precipitation, with the exception of Sichuan, which increased a little (+0.65 mm/decade) from the 1970s to 2010s (Fig. 5(c)).

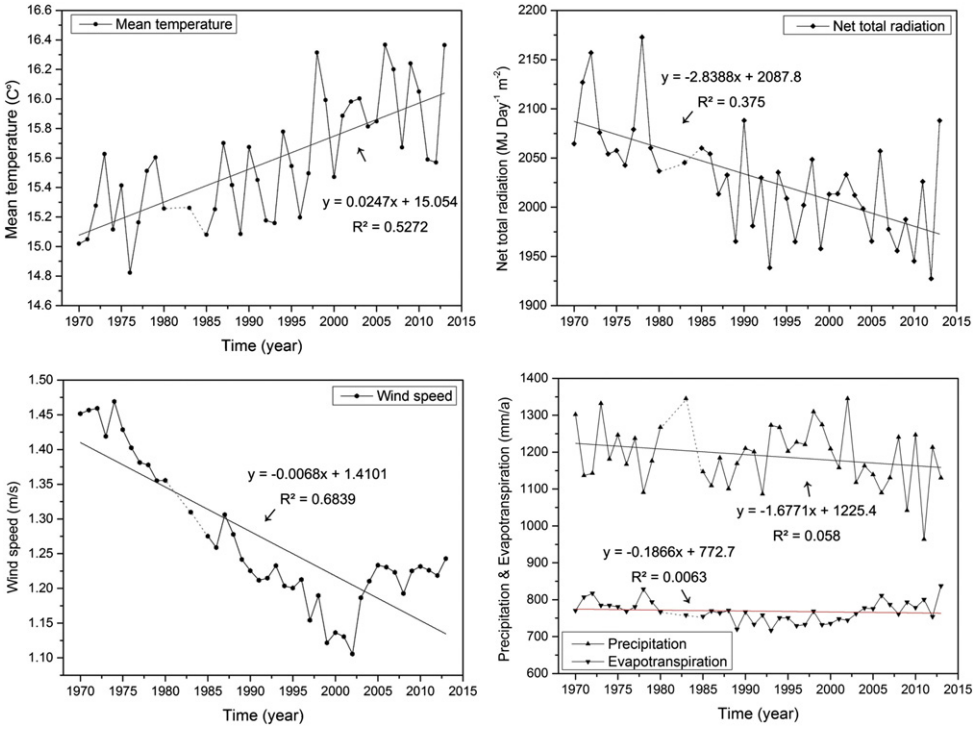

Fig. 4. Annual mean value and trends of temperature (T_{mean}), net total radiation (R_n), wind speed (WS), precipitation (P) and evapotranspiration (ET) of the 240 meteorological stations in and around SW China from 1970 to 2013 (dotted line: data missing).

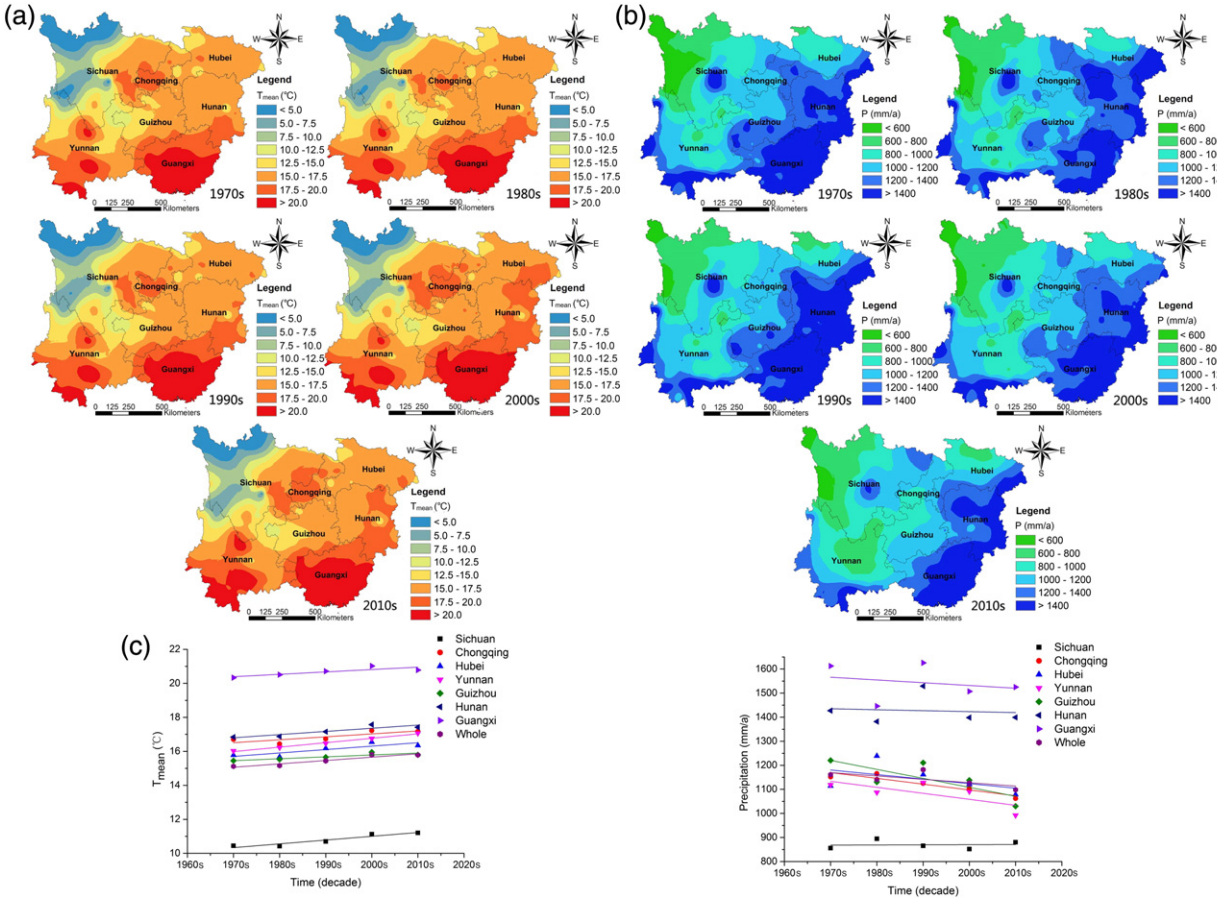

Fig. 5. Spatial distribution and temporal trends of mean temperature and precipitation in SW China from 1970s to 2010s.

4.2. Spatial – temporal distribution of runoff depth

As shown in Fig. 6, the annual *D* varied from 200 mm to 1200 mm with an average of 386 mm. Distribution of annual *D* values demonstrated a strong spatial gradient, with higher values in the southeast (Guangxi, Hunan) and lower values in the western part of the study area (Sichuan, Yunnan). Meanwhile, the annual *D* values in the 2010s were significantly lower than other periods, with the lowest values found in Yunnan and Guizhou provinces.

Table 2 shows the mean values of climate parameters and runoff depth (*D*) in different time periods in the SW China karst region. It is noteworthy that precipitation and *ET* reached extreme values in 1990s, as much as 1188 mm and as low as 754 mm (Table 2), respectively. The mean annual *D* in the karst region showed an overall decreasing trend (about 18% decrease), with an anomaly in the 1990's when the highest *D* occurred (444 mm/a); the lowest *D* (308 mm/a) in 2010s.

4.3. Spatial – temporal distribution of equilibrium HCO_3^- concentration

Equilibrium concentrations of the HCO_3^- in the karst region with different types of carbonate rocks were calculated by using MPD and Eq. (3) (modified MPD). The average $[HCO_3^-]_{eq}$ values of limestone and dolomite were used to present the equilibrium concentration of mixed limestone/dolomite and impure carbonate under different conditions of temperature and pCO_2. The mean temperature and soil pCO_2 are significant controlling factors of $[HCO_3^-]_{eq}$ in the modified MPD. The annual mean soil pCO_2 was calculated by the Brook's formula (Brook et al., 1983). The decade mean values of soil pCO_2 varied from 11,290 ppmv to 12,520 ppmv (Table 2). The equilibrium concentrations of bicarbonate based on temperature and soil pCO_2 are shown in Fig. 7.

The mean $[HCO_3^-]_{eq}$ value is 4.29 mmol/L in the karst region of SW China, of which the highest and lowest values were observed in the western and eastern parts, respectively. The $[HCO_3^-]_{eq}$ in the western portion of the karst region increased only slightly with climate change. In the central region, however, there was a remarkable change of $[HCO_3^-]_{eq}$, decreasing from 1970s to 1990s and increasing after 2000s. The $[HCO_3^-]_{eq}$ concentrations for each type of carbonate in the study periods are shown in Table 2, with 4.01, 5.01, 4.58, and 4.63 (mmol/L) for limestone, dolomite, mixed limestone/dolomite and impure carbonate, respectively. These average equilibrium concentrations for different types of carbonates changed only slightly (<5%) over the study periods despite the changing climate conditions. In all types of carbonates, the highest and lowest $[HCO_3^-]_{eq}$ occurred in 1970s (5.12 mmol/L for dolomite) and 1990s (3.92 mmol/L for limestone), respectively.

4.4. Spatial – temporal distribution of CSFs

Based on the modified MPD formula and GIS spatial calculation, the annual mean total carbon sink (TCS) of the SW China karst region was obtained, which was 68.9×10^5 t C. Guangxi, Guizhou, Hunan, Yunnan, Hubei, Sichuan and Chongqing contributed 22.86%, 22.61%, 20.46%, 11.78%, 8.5%, 8.29%, and 5.52% to the total TCS in the study area, respectively. Distribution of annual CSFs also demonstrated the same strong

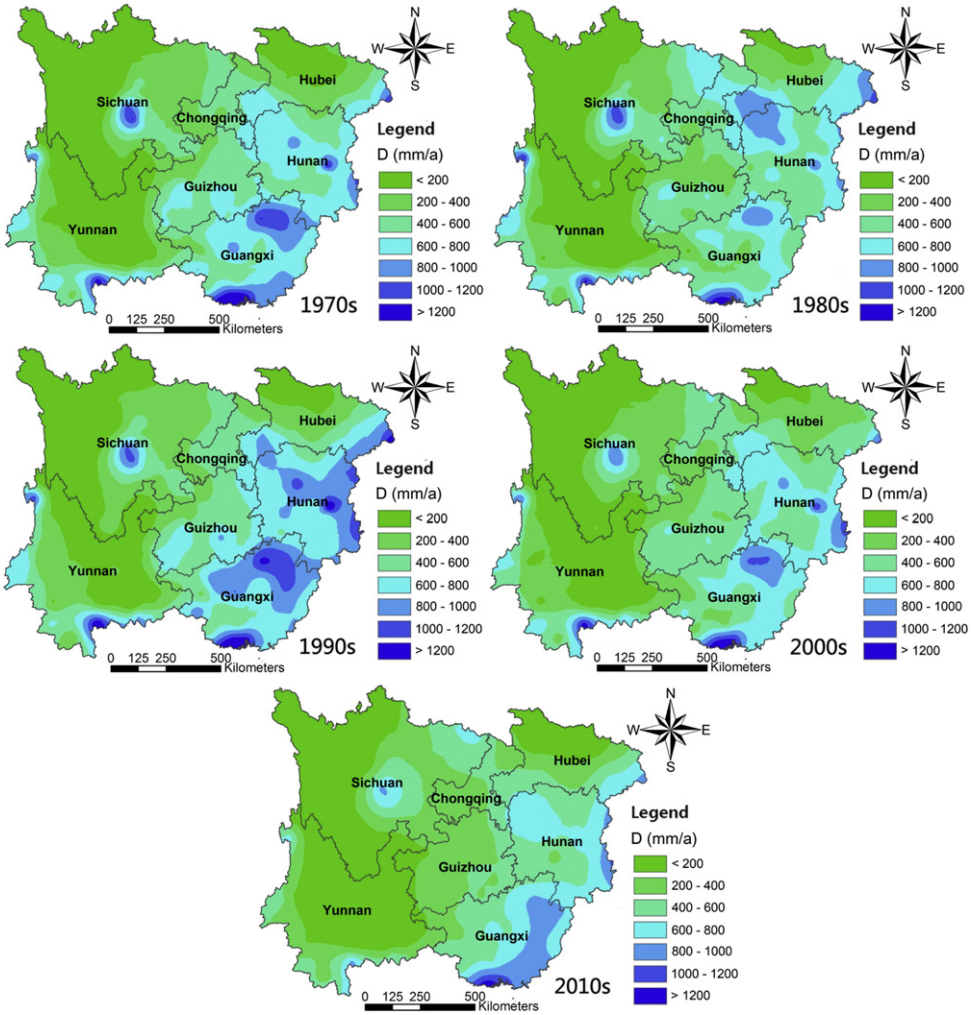

Fig. 6. Spatial distribution of runoff depth (*D*) in SW China from 1970s to 2010s.

Table 2
Decade mean values of temperature (T_{mean}), precipitation (P), evapotranspiration (ET), runoff depth (D), soil CO_2 and equilibrium HCO_3^- concentrations of limestone [$(Ceq)_L$], dolomite [$(Ceq)_D$], mixed limestone/dolomite [$(Ceq)_{L/D}$], and impure carbonate [$(Ceq)_I$] in the SW China karst region from 1970s to 2010s.

Period	T_{mean}	P	ET	D	pCO_2	$(Ceq)_L$	$(Ceq)_D$	$(Ceq)_{L/D}$	$(Ceq)_I$
	(°C)	(mm/a)	(mm/a)	(mm/a)	(ppmv)	(mmol/L)	(mmol/L)	(mmol/L)	(mmol/L)
1970s	15.28	1172	802	394	12,481	4.09	5.12	4.65	4.75
1980s	15.35	1130	776	373	11,852	4.01	5.01	4.57	4.63
1990s	15.60	1188	754	444	11,290	3.92	4.90	4.47	4.54
2000s	15.96	1123	778	360	11,889	3.95	4.94	4.50	4.58
2010s	15.95	1075	803	308	12,520	4.01	5.06	4.57	4.65

spatial gradient as runoff depth (D), with higher CSFs values in the east and lower values in the west (Fig. 8). The CSFs in central of Sichuan, northeast of Guangxi, east of Hunan were particularly high (Fig. 8). In 1990s, the CSFs in Guangxi, Hunan, Guizhou were the highest. In 2010s, however, there was a remarkable decrease in the CSFs in Sichuan and Guizhou provinces, as shown in Fig. 8. The effect of climate change on TCS is that there was, overall, a 19% decrease in the entire karst region of SW China from 1970s to 2010s.

5. Discussion

5.1. Comparison with other methods

MPD is a theoretical calculation of optimized carbonate dissolution assuming a steady rate of change. It corresponds, physically, to the theoretical carbonate rock layer dissolved by karstic processes in the basin catchment area. It is necessary to check for similarity between the MPD-based results and those by other methods of calculating carbonate dissolution rates. As shown in Table 3, the calculated karst-related carbon sink fluxes (CSFs) in SW China, based on the modified MPD formula, ranged from 7.4 to 10.4 t C km^{-2} a^{-1} (or 27.1 to 38.1 t CO_2 km^{-2} a^{-1}) from 1970s to 2010s, and the average CSFs in SW China was 9.36 t C km^{-2} a^{-1}. To assess the results of the MPD method, we compared the modified MPD-based results with those by other methods (Table 4). Results show that the CSFs are mostly within 5% of each other, with only one exception still being within 20%. For example, the CSFs in upper reaches of Xijiang River (tributary catchments of the Pearl River) was 27.05 t CO_2 km^{-2} a^{-1}, based on the solute load method by Xu and Liu et al. (2007), while the CSFs obtained from the modified MPD was 27.75 t CO_2 km^{-2} a^{-1}. A high-resolution (15 min interval),

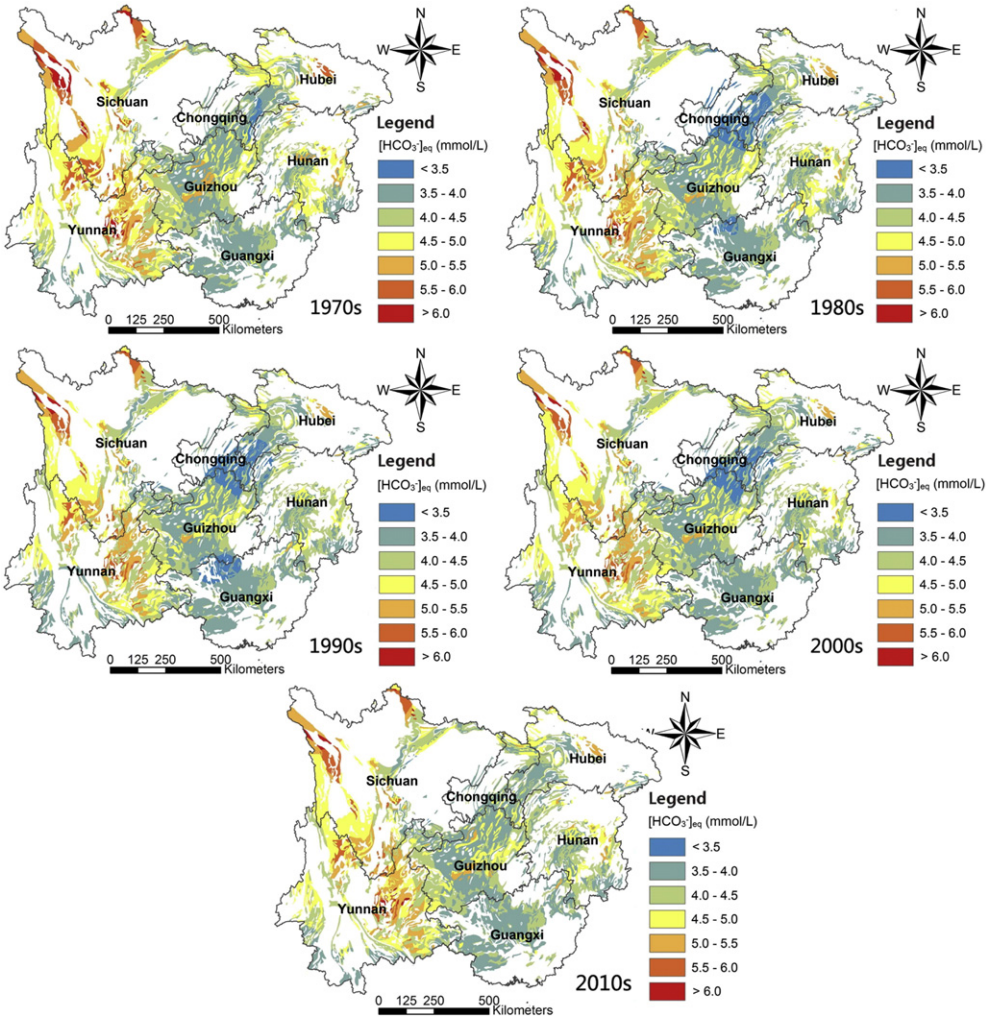

Fig. 7. Spatial distribution of equilibrium HCO_3^- concentration $[HCO_3^-]_{eq}$ in SW China karst area from 1970s to 2010s.

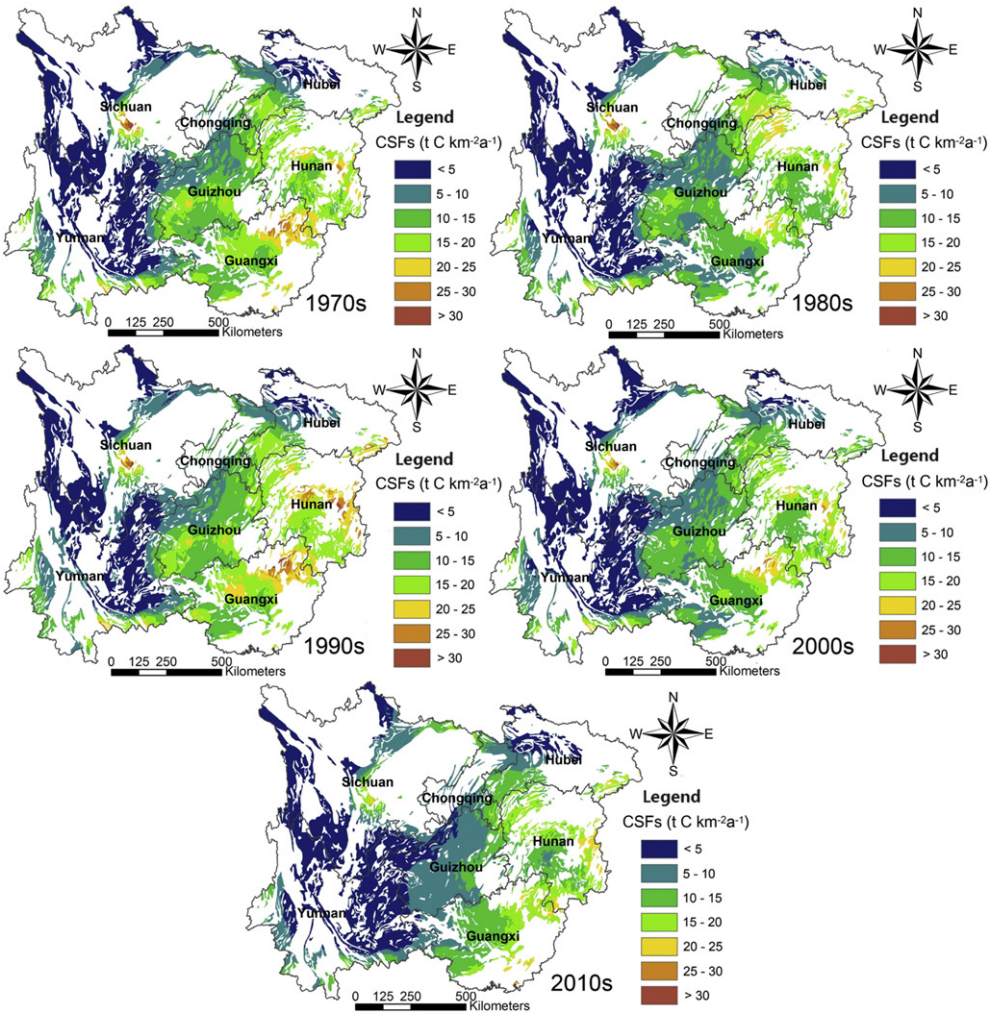

Fig. 8. Spatial distribution of the karst-related carbon sink fluxes (CSFs) in SW China from 1970s to 2010s.

Table 3
Statistics on the temporal variations in mean temperature (T_{mean}), runoff depth (D), equilibrium HCO_3^- concentration $[HCO_3^-]_{eq}$, carbon sink flux ($CSFs$), and total carbon sink (TCS) in the seven provinces of SW China from 1970s to 2010s.

Decade	Items	Sichuan	Chongqing	Hubei	Yunnan	Guizhou	Hunan	Guangxi	SW China
1970s	T_{mean} (°C)	10.21	16.00	15.62	15.29	15.36	16.99	20.23	15.28
	D (mm/a)	104	444	313	215	498	646	747	394
	$[HCO_3^-]_{eq}$ (mmol/L)	4.60	3.80	4.00	4.48	4.00	4.12	3.78	4.21
	$CSFs$ (t C km^{-2} a^{-1})	3.8	12.1	9.0	4.7	11.9	17.3	16.7	9.6
	TCS (10^5t C)	5.4	3.9	5.3	8.9	17.2	14.2	17.2	72.1
1980s	T_{mean} (°C)	10.23	15.79	15.43	15.46	15.45	17.04	20.42	15.35
	D (mm/a)	184	538	556	181	428	616	532	374
	$[HCO_3^-]_{eq}$ (mmol/L)	4.75	3.87	4.00	4.59	4.07	4.22	3.88	4.30
	$CSFs$ (t C km^{-2} a^{-1})	4.7	13.5	12.4	4.3	10.2	15.9	12.6	8.9
	TCS (10^5t C)	6.6	4.3	7.3	8.2	14.7	13.1	12.9	67.1
1990s	T_{mean} (°C)	10.58	16.10	15.88	15.72	15.58	17.30	20.60	15.60
	D(mm/a)	176	490	467	229	520	780	767	444
	$[HCO_3^-]_{eq}$ (mmol/L)	4.64	3.86	4.00	4.47	4.00	4.12	3.78	4.21
	$CSFs$ (t C km^{-2} a^{-1})	4.5	12.1	10.3	5.4	12.1	19.7	17.7	10.4
	TCS (10^5t C)	6.3	3.9	6.1	10.2	17.6	16.2	18.2	78.5
2000s	T_{mean} (°C)	11.02	16.62	16.22	16.04	15.85	17.69	20.91	15.96
	D(mm/a)	172	453	426	172	430	629	589	360
	$[HCO_3^-]_{eq}$ (mmol/L)	4.64	3.89	4.04	4.52	4.02	4.17	3.85	4.25
	$CSFs$ (t C km^{-2} a^{-1})	3.7	11.4	9.6	4.0	10.1	16.1	13.9	8.5
	TCS (10^5t C)	5.2	3.7	5.7	7.8	14.6	13.2	14.3	64.5
2010s	T_{mean} (°C)	11.13	16.53	16.04	16.33	15.69	17.55	20.67	15.95
	D(mm/a)	156	373	343	106	259	601	596	308
	$[HCO_3^-]_{eq}$(mmol/L)	4.70	4.02	4.13	4.60	4.11	4.26	3.84	4.32
	$CSFs$ (t C km^{-2} a^{-1})	4.0	9.8	7.8	2.5	7.1	15.7	14.0	7.4
	TCS (10^5t C)	5.6	3.1	4.6	4.7	10.2	12.9	14.4	55.5

Table 4
Comparison of the karst-related carbon sink fluxes (t CO_2 $km^{-2}a^{-1}$) between the MPD-based results and those by other methods.

Site	Upper Xijiang R.	Guizhou 1	Guizhou 2	Yangtze R.	Pearl R.
Other studies	27.05[a]	28.84[b]	39.13[b]	38.75[c]	42.7[d]
This study	27.75	33.9	38.62	40.15	45.32
Ratio, this to other	1.03	1.18	0.99	1.04	1.06

[a] Xu and Liu, 2007.
[b] Zeng et al., 2016.
[c] Han and Liu, 2004.
[d] Cao et al., 2011.

monitoring-based CSFs estimation of the three catchments in Guizhou ranged from 28.84 to 39.13 t CO_2 km^{-2} a^{-1} during the period of 2007 to 2013 (Zeng et al., 2016), while the CSFs obtained from the modified MPD ranged from 33.90 to 38.62 t CO_2 km^{-2} a^{-1} in these three catchments from 2007 to 2013.

In addition, Han and Liu (2004) measured the water chemistry in numerous tributary catchments of the Yangtze River in Guizhou province and the CSFs of these catchments was 38.75 t CO_2 $km^{-2}a^{-1}$, which is close to our calculation (40.15 t CO_2 $km^{-2}a^{-1}$). The karst-related carbon sink flux in the Pearl River Basin in SW China was about 42.70 t CO_2 km^{-2} a^{-1} by Cao et al. (2011) who used a regression equation containing major impact factors of karst processes (solution ratio of standard limestone tablets, precipitation, soil respiration and NPP), which is also close to our MPD-based result (45.32 t CO_2 $km^{-2}a^{-1}$).

All these comparisons show that the modified MPD method is as effective as other methods in calculating the karst-related carbon sink fluxes. This also indicates that maximum potential carbonate dissolution has been maintained in nature due to the fast dissolution kinetics of carbonate rocks (Dreybrodt, 1988; Gombert, 2002; Liu et al., 2010; Liu et al., 2011).

5.2. Runoff depth: the major factor determining the carbonate weathering-related carbon sink

The relationships between carbon sink flux (CSFs) and precipitation, temperature, runoff depth (D), or $[HCO_3^-]_{eq}$ of the whole karst region in SW China from 1970s to 2010s are shown in Fig. 9. There is a strong positive relationship between CSFs and D or precipitation, but no significant relationship between CSFs and mean temperature or $[HCO_3^-]_{eq}$. This suggests that the variation in CSFs is mainly controlled by precipitation or D during the study period, and the influence of temperature and $[HCO_3^-]_{eq}$ on CSFs variations can be ignored. Furthermore, a comparison is provided in Table 3 and Fig. 10 for the seven provinces in SW China in the study period. It can be seen that, in the whole study period, the largest decrease in CSFs occurred in Guizhou (−37%) and Yunnan (−32%). During the same time period, these two provinces experienced a similar decrease in D (190 mm and 90 mm decrease in the past 40 years, respectively) and precipitation (156 mm and 106 mm in the past 40 years, respectively). However, there was an increase in air temperature (0.33 and 1.04 °C increase over the past 40 years, respectively) and $[HCO_3^-]_{eq}$ in the karst regions of Guizhou and Yunnan. Fig. 10 also demonstrates that the trends of decreasing TCS and CSFs among the provinces were similar. More important is that a synchronous trend was found between CSFs and D, but a reversed trend was observed between CSFs and $[HCO_3^-]_{eq}$ (Fig. 10), indicating that runoff depth was the major factor determining the karst-related carbon sink.

According to multiple linear regression analysis, the karst-related carbon sink fluxes can be approximated by the following equation:

$$CSFs = 10.423 + 0.021D - 2.184[HCO_3^-]_{eq},\ R^2 = 0.987, p<0.01, \quad (6)$$

where CSFs is the karst-related carbon sink, D is the runoff depth (mm/a), and $[HCO_3^-]_{eq}$ (mmol/L) is the equilibrium bicarbonate concentration under local climate conditions.

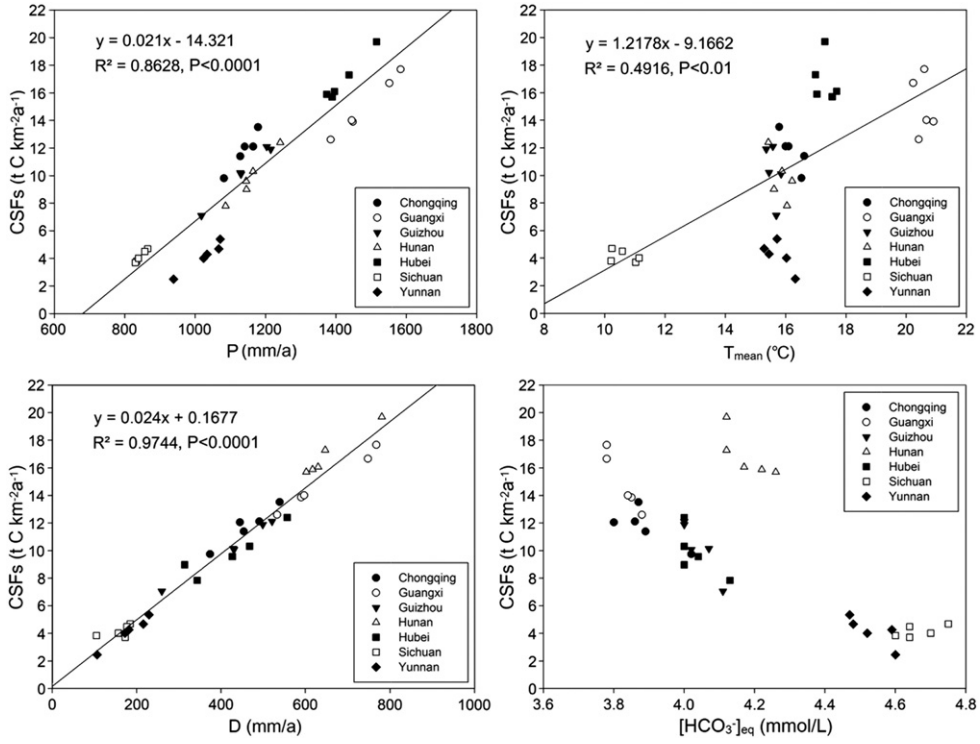

Fig. 9. Relationship between carbon sink flux (CSFs) and precipitation, mean temperature, runoff depth (D), or $[HCO_3^-]_{eq}$ of the seven provinces in SW China from 1970s to 2010s.

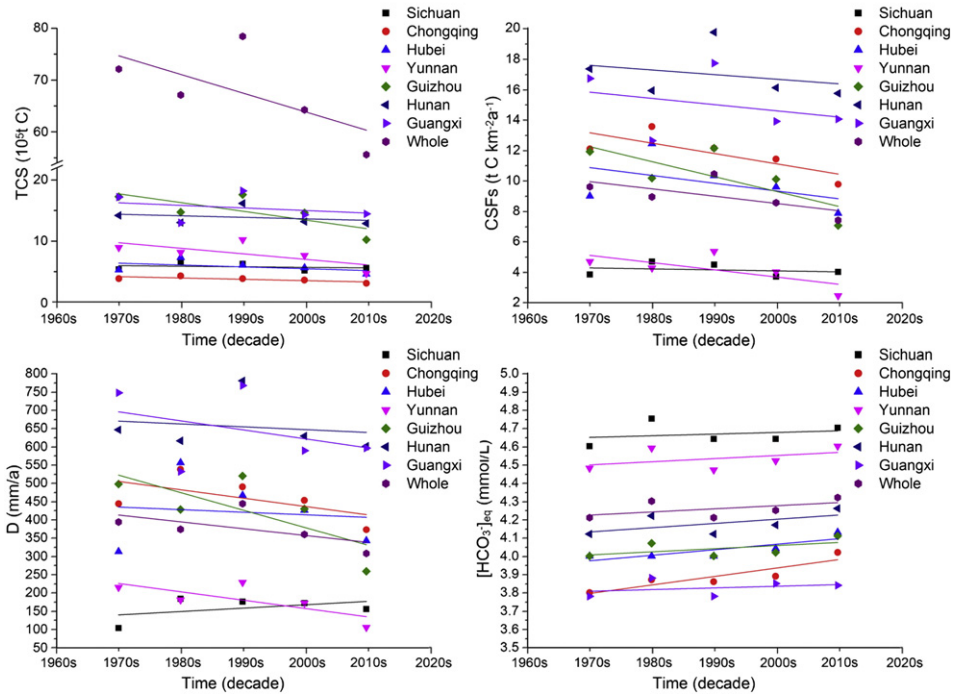

Fig. 10. Variations in total carbon sink (TCS), carbon sink flux (CSFs), runoff depth (D) and equilibrium HCO_3^- concentration $[HCO_3^-]_{eq}$ in the seven provinces and entire SW China karst area from 1970s to 2010s.

The strong positive correlation between CSFs and D but not $[HCO_3^-]$ found in SW China was consistent with field observations (Godsey et al., 2009; Clow and Mast, 2010; Zeng et al., 2016), in which the chemostatic behavior of $[HCO_3^-]$ was found. The chemostatic behavior in catchments means that concentration of weathering products in streams often show relatively little variation compared to changes in discharge, both at storm and interannual timescales (Godsey et al., 2009; Clow and Mast, 2010). The mechanisms for the chemostatic behavior of $[HCO_3^-]$ in karst catchments may include two controls (Zeng et al., 2016). One is that the decrease in $[HCO_3^-]$ is caused by simple dilution is counterbalanced by an increase in $[HCO_3^-]$ induced by a soil CO_2 effect (Liu et al., 2007) in the rainy periods. The second is the fast kinetics of carbonate dissolution, which overcomes the dilution effect by the discharge increase after a rainfall (the so-called transport-limited behavior, Maher, 2010). This is the reason why there were high similarities in variation patterns between CSFs and D in all provinces from 1970s to 2010s (Fig. 10).

5.3. Comparison of carbon sink fluxes among the provinces: difference in climate and carbonate lithologies

According to Eq. (1) and Eq. (6), the carbon sink flux is determined by D and $[HCO_3^-]_{eq}$. Therefore, as shown in Table 3, Hunan Province had the highest CSFs among the seven provinces due to its highest D (666 mm/a) and a larger area of dolomite and mixed limestone/dolomite distribution (Fig. 2), with thus higher $[HCO_3^-]_{eq}$ (Table 3).

Sichuan and Yunnan had higher $[HCO_3^-]_{eq}$ (Table 3) among the seven provinces. However, their lowest D (159 mm/a and 181 mm/a, respectively) contributed the lowest carbon sink fluxes in these two provinces. The main reason for the CSFs difference among provinces is the regional climate difference. Most of the area in Yunnan, Guizhou, and Sichuan are mountains and Plateaus (Tibet Plateau and Yunnan-Guizhou plateau), thus having higher average elevation, as illustrated in Fig. 1. The provinces in southeast of SW China, however, are mainly dominated by plains and are more strongly affected by the monsoonal climate. Therefore, the area of southeast thus has more rainfall than the northwest.

5.4. Implication for the carbon cycle

It has been shown that the CSF in SW China karst area is 9.36 t C km^{-2} a^{-1} (or 34.3 t CO_2 km^{-2}a^{-1}), which is about 18 times larger than that in a silicate-dominated terrain (about 1.94 t CO_2 km^{-2}a^{-1}, Jin et al., 2014). Moreover, the carbon sink produced by carbonate weathering was sensitive to climate change, due to the runoff effect determined by the transport-limited behavior of carbonate weathering (as evidenced by the chemostatic behavior of $[HCO_3^-]$ shown earlier). For example, the karst-related carbon sink showed a 19% decrease due to the decrease in runoff depth in SW China from 1970 to 2013. Therefore, this study suggests that there will be a rapid response of the karst-related carbon sink to future climate change, which needs to be considered in the modern global carbon cycle study. Huntington (2006) had shown the evidence for intensification of the global water cycle (2–5% increase per degree) due to global warming, so there will be an increase in the karst-related carbon sink (Liu et al., 2010). Though Bond-Lamberty and Thomson (2010) showed that soil respiration rates have increased (~0.1% in the past 20 years from 1989 to 2008) because of climate warming, the dependence of CSF on $[HCO_3^-]$ was minor due to much weaker increase in $[HCO_3^-]$ than runoff increase.

6. Conclusion

Based on the modified MPD formula and GIS, this study used daily climatic data from the 240 meteorological stations during 1970–2013 and distribution of various carbonate rocks in SW China to analyze perturbations of karst-related carbon sink under changed climate conditions. We focused on four aspects: (1) spatiotemporal variations of the main determinants controlling the carbon sink fluxes, (2) spatiotemporal variations of the total karst-related carbon sink (TCS) and carbon fluxes (CSFs), (3) climatic impacts on the CSFs variations, and (4) possible implications of this study.

It was found that the TCS in SW China experienced a dramatic change with regional climate, and there was a trend with TCS

decreasing by about 19% from 1970 to 2013. This decrease occurred mostly in Guizhou and Yunnan provinces, which experienced larger decreases in runoff depth (190 mm and 90 mm in the past 40 years, respectively) due to increased air temperature (0.33 °C and 1.04°Cin the past 40 years, respectively) and decreased precipitation (156 mm and 106 mm in the past 40 years, respectively) in the karst region during the same period. The mean value of CSFs in SW China, calculated by the modified MPD method, was approximately 9.36 t C km^{-2} a^{-1}. In addition, there were large differences in CSFs among the provinces, attributed to the difference in regional climate and carbonate lithologies. These spatiotemporal changes depended mainly on the hydrological variations (i.e., discharge or runoff depth) in the karst regions during climate changes over about 40 years. Thus, this study suggests that the karst-related carbon sink could respond to future climate change quickly, and needs to be considered in the modern global carbon cycle model.

Acknowledgements

This research was supported by the Ministry of Science and Technology of China (2016YFC0502306 and 2013CB956700) and the National Science Foundation of China (41430753, 41472321 and 41172331). Special thanks are given to Prof. G.L. Macpherson for her thoughtful academic and editorial suggestions on the manuscript.

References

Allen, R.G., Pereira, L.S., Raes, D., Smith, M., 1998. Crop evapotranspiration: Guideline for computing crop water requirement. FAO Irrigation and Drainage Paper No.56. Food and Agriculture Organization, Italy.

Andrews, J.A., Schlesinger, W.H., 2001. Soil CO_2 dynamics, acidification, and chemical weathering in a temperate forest with experimental CO_2 enrichment. Glob. Biogeochem. Cycles 15, 149–162.

Berner, R.A., 1992. Weathering, plants, and the long-term carbon cycle. Geochim. Cosmochim. Acta 56, 3225–3231.

Berner, R.A., Lasaga, A.T., Garrels, R.M., 1983. The carbonate-silicate geochemical cycle and its effect on atmospheric carbon dioxide over the past 100 million years. Am. J. Sci. 283, 641–683.

Bond-Lamberty, B., Thomson, A., 2010. Temperature-associated increases in the global soil respiration record. Nature 464, 579–582.

Brook, G.A., Folkoff, M.E., Box, E.O., 1983. A world model of soil carbon dioxide. Earth Surf. Process. Landf. 8, 79–88.

Cao, J.H., Yang, H., Kang, Z.Q., 2011. Preliminary regional estimation of carbon sink flux by carbonate rock corrosion: a case study of the Pearl River basin. Chin. Sci. Bull. 56, 3766–3773.

Clow, D.W., Mast, M.A., 2010. Mechanisms for chemostatic behavior in catchments: implications for CO_2 consumption by mineral weathering. Chem. Geol. 269, 40–51.

Drever, J.I., 1994. The effect of land plants on weathering rates of silicate minerals. Geochim. Cosmochim. Acta 58, 2325–2332.

Dreybrodt, W., 1988. Processes in Karst Systems. Springer Series in Physical Environment. Springer, Heidelberg.

Friedlingstein, P., Cox, P., Betts, R., 2006. Climate-carbon cycle feedback analysis: results from the (CMIP)-M-4 model intercomparison. J. Clim. 14, 3337–3353.

Gedney, N., Cox, P.M., Betts, R.A., 2006. Detection of a direct carbon dioxide effect in continental river runoff records. Nature 439, 835–838.

Gislason, S.R., Oelkers, E.H., Eiriksdottir, E.S., 2009. Direct evidence of the feedback between climate and weathering. Earth Planet. Sci. Lett. 277, 213–222.

Godsey, S.E., Kirchner, J.W., Clow, D.W., 2009. Concentration-discharge relationships reflect chemostatic characteristics of US catchments. Hydrol. Process. 23, 1844–1864.

Gombert, P., 2002. Role of karstic dissolution in global carbon cycle. Glob. Planet. Chang. 33, 177–184.

Han, G., Liu, C., 2004. Water geochemistry controlled by carbonate dissolution: a study of the river waters draining karst-dominated terrain, Guizhou Province, China. Chem. Geol. 204, 1–21.

Huntington, T.G., 2006. Evidence for intensification of the global water cycle: review and synthesis. J. Hydrol. 319, 83–95.

Jin, L., Ogrinc, N., Yesavage, T., Hasenmueller, E.A., Ma, L., Sullivan, P.L., Kaye, J., Duffy, C., Brantley, S.L., 2014. The CO_2 consumption potential during gray shale weathering: insights from the evolution of carbon isotopes in the Susquehanna Shale Hills critical zone observatory. Geochim. Cosmochim. Acta 142, 260–280.

Liu, Z., Dreybrodt, W., 2015. Significance of the carbon sink produced by H_2O–carbonate–CO_2–aquatic phototroph. Sci. Bull. 60, 182–191.

Liu, Z., Zhao, J., 2000. Contribution of carbonate rock weathering to the atmospheric CO_2 sink. Environ. Geol. 39, 1053–1058.

Liu, Z., Li, Q., Wang, J., 2007. Seasonal, diurnal and storm-scale hydrochemical variations of typical epikarst springs in subtropical karst areas of SW China: soil CO_2 and dilution effects. J. Hydrol. 337, 207–223.

Liu, Z., Dreybrodt, W., Wang, H., 2010. A new direction in effective accounting for the atmospheric CO_2 budget: considering the combined action of carbonate dissolution, the global water cycle and photosynthetic uptake of DIC by aquatic organisms. Earth-Sci. Rev. 99, 162–172.

Liu, Z., Dreybrodt, W., Liu, H., 2011. Atmospheric CO_2 sink: silicate weathering or carbonate weathering? Appl. Geochem. 26s, 292–294.

Macpherson, G.L., Roberts, J.A., Blair, J.M., Townsend, M.A., Fowle, D.A., Beisner, K.R., 2008. Increasing shallow groundwater CO_2 and limestone weathering, Konza Prairie, USA. Geochim. Cosmochim. Acta 72, 5581–5599.

Maher, K., 2010. The dependence of chemical weathering rates on fluid residence time. Earth Planet. Sci. Lett. 294, 101–110.

Melnikov, N., O'Neill, B., 2006. Learning about the carbon cycle from global budget data. Geophys. Res. Lett. 33, L02705.

Raymond, P.A., Cole, J.J., 2003. Increase in the export of alkalinity from North America's Largest River. Science 301, 88–91.

Raymond, P.A., Oh, N.H., Turner, R.E., Broussard, W., 2008. Anthropogenically enhanced fluxes of water and carbon from the Mississippi River. Nature 451, 449–452.

Sabine, C.L., et al., 2004. Current status and past trends of the carbon cycle. In: Field, C.B., Raupach, M.R. (Eds.), The Global Carbon Cycle: Integrating Humans, Climate, and the Natural World. Island Press, Washington, pp. 17–44.

Tans, P.P., Fung, I.Y., Takahashi, T., 1990. Observational constraints on the global atmospheric CO_2 budget. Science 247, 1431–1438.

Xu, Z., Liu, C., 2007. Chemical weathering in the upper reaches of Xijiang River draining the Yunnan-Guizhou Plateau, Southwest China. Chem. Geol. 239, 83–95.

Yang, R., Liu, Z., Zeng, C., Zhao, M., 2012. Response of epikarst hydrochemical changes to soil CO_2 and weather conditions at Chenqi, Puding, SW China. J. Hydrol. 468–469, 151–158.

Yin, Y., Wu, S., Zheng, D., 2008. Radiation calibration of FAO56 Penman-Monteith model to estimate reference crop evapotranspiration in China. Agric. Water Manag. 95, 77–84.

Yuan, D., 1997. The carbon cycle in karst. Zeitschrift fur Geomorphologie 108, 91–102 (NF).

Zeng, C., Liu, Z., Zhao, M., Yang, R., 2016. Hydrologically-driven variations in the karst-related carbon sink fluxes: insights from high-resolution monitoring of three karst catchments in Southwest China. J. Hydrol. 533, 74–90.